Integration of multicomponent processing and interpretation of the Pouce Coupe time-lapse survey: focus on shear-wave splitting analysis

Jeff P. Grossman and Gulia Popov, Sensor Geophysical, Chris Steinhoff, Colorado School of Mines*

Summary

Multicomponent seismic processing and interpretation have become disconnected in industry practice, hindering the ability to extract meaningful reservoir characterization conclusions. Integrating seismic processing with the final interpretation goals elevates seismic characterization and drives advancements in processing algorithms. The focus of this study was on seismic characterization using converted-waves (C-waves) because of their high sensitivity to the azimuthal anisotropy caused by preferential fractures and differential stress, and ultimately because they provide a method of correlating hydraulic stimulation success to the enhanced permeability pathways created in the hydraulic completion process.

This study combines the processing and interpretation of the Pouce Coupe time-lapse (4D) multicomponent (3C) surveys (Figure 1), investigating hydraulic stimulations of two horizontal wells targeting the Montney shale. Due to unsatisfactory processing results the data set was reprocessed utilizing new methods to better preserve vector fidelity, improve prestack shear-wave splitting (SWS) analysis and layer stripping, and enhance 4D repeatability. The updated results show a strong correlation between the magnitude and orientation of seismically derived induced reservoir azimuthal anisotropy and individual stage production. The baseline characterization provides a strong argument that drilling and completion practices should be driven by interpretation of the local scale reservoir complexities that can improve completion success.

Introduction

The Pouce Coupe 4D 3C data provide insight into stress and fracture-related reservoir shear-wave anisotropy through the analysis of SWS. Atkinson and Davis (2011) found promising results relating to shear-wave seismic anisotropy changes within the Montney shale when they analyzed these same seismic surveys, but concluded the previous processing was inadequate and required technical improvements before meaningful reservoir characterization solutions could be extracted.

In response, the data have been reprocessed and this study outlines the technical developments that have been made since then on integrative methods of processing and interpretation as a consequence of focusing our objective on azimuthal anisotropy characterization. Specifically, on the processing side, we discuss receiver azimuth detection and rotation (RADAR), simultaneous NRMS (normalized root mean squared)-guided processing, and maximization of coherence of the radial component for SWS analysis of common azimuth stacks. Interpretation of azimuthal anisotropy within the reservoir interval was determined poststack using SWS analysis, quantified by the time delays between fast and slow shear travel times of the base of reservoir event (Martin and Davis, 1987). The baseline (pre hydraulic stimulation) was interpreted for insitu reservoir conditions and two hydraulic fracture stimulations were monitored to determine the induced azimuthal anisotropy. The azimuthal anisotropy responses were then linked to production log data quantifiying the contribution of hydrocarbon flow from individual stage locations.

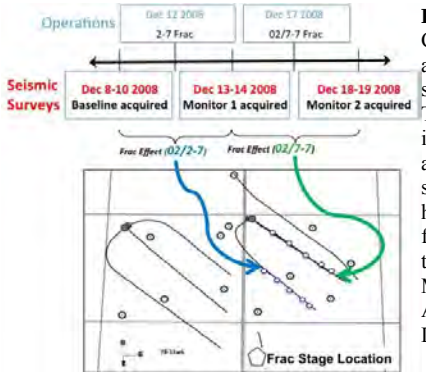

Figure 1. Pouce Coupe operations and 4D 3C seismic timeline. The seismic data include a baseline and two monitor surveys over two horizontal well fracturing treatments. Modified from Atkinson and Davis (2011).

Processing

Certain important 3C processing and quality control algorithms such as SWS analysis and layer stripping tacitly rely on vector fidelity of the recording to be maintained and for this reason have often failed to provide reliable results. Fundamental processing improvements such as those we present below enable more sophisticated algorithms, and thus additional information to be accurately extracted from seismic data.

RADAR. RADAR, a recently developed high-fidelity method for automatically detecting and correcting receiver azimuths, (Grossman and Couzens, 2012) addresses vector infidelity problems—ultimately caused by errors in the reported receiver azimuth—which arise during rotation of the laterally polarized data measurements from the acquisition coordinates into orthogonal radial (R) and transverse (T) coordinates (Gaiser, 1999). Such errors cause undesirable 'leakage' of R energy onto the T component, which can be misinterpreted as evidence of SWS (Cary, 2002) or out-of-plane reflection energy.

The impact of RADAR on the Pouce Coupe converted-wave data is illustrated by the reduction of coherent energy on the T component, with/without RADAR in Figure 2. All four receiver gathers are T component data, and each column corresponds to a different receiver station location. The bottom row demonstrates a large amount of T energy

remaining after rotation to the reported azimuth, and the top row shows reduced T energy after RADAR. Energy from shear-mode head waves (in the lower left-hand corner) is also much weaker and less coherent in the RADAR results. Additional evidence in support of RADAR is provided by examination of the common receiver stacks in Figure 3.

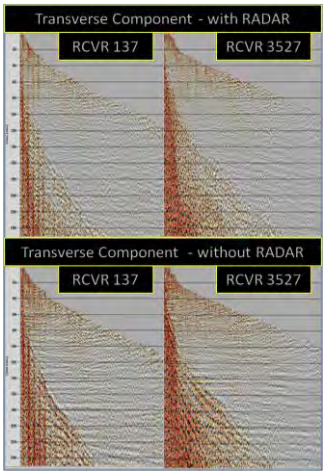

Figure 2. Transverse component receiver gathers at two locations (one per column), rotated from field coordinates using two different angles: 1) the RADAR-detected azimuth (top row) and 2) the reported azimuth (bottom row). The greater reduction of both reflection and shear refraction energy for RADAR shows an improvement in vector fidelity, as coherent energy is normally not expected to appear on the transverse component.

Successful rotation to R and T coordinates using the correct azimuth led to many improvements in the processing, including SWS analysis and layer stripping results, and more generally with regard to enhanced repeatability across the baseline and both monitors. Repeatability was also enhanced by incorporating the simultaneous NRMS-guided time-lapse processing methodology of Li, et al. (2012).

Time-lapse processing. The data were processed for the highest repeatability, allowing for any 4D effects within the reservoir to be interpreted as physical changes in reservoir properties. The repeatability-focused acquisition design included permanent placement of geophones, making it an ideal candidate for reservoir monitoring.

Time-lapse repeatability was improved by processing the multiple vintage seismic surveys simultaneously (Lumley et al., 2003) while carefully preserving information content. Reflection signal from the no-change zones—where 4D effects are not expected—was monitored using NRMS as a repeatability metric (Kragh and Christie, 2002). Throughout processing, NRMS error is measured in the no-change zones and a step is accepted only if NRMS error decreases or is at least maintained from the previous step. This enhancement to simultaneous processing makes repeatability monitoring viable throughout the processing sequence rather than with a single reconciliation effort at the end, also alleviating the need for potentially deleterious processes such as poststack cross-equalization. This methodology is discussed in detail by Li, et al. (2012).

Following the interpretation of the baseline natural fractures, the reservoir was monitored by the consecutive acquisition of seismic surveys after hydraulic fracturing treatments (Figures 1 and 7). Careful processing of the 4D 3C data resulted in higher interpretation confidence within the reservoir interval. The NRMS error was found to decrease significantly over that of the former processing, due to the initial treatment of the receiver azimuths pre-processing, improving the signal-to-noise ratio and the resolved statics (Figure 4). Confidence in the 4D anomalies only exists in the highest repeatability areas; thus, interpretation is focused on the polygon section on the NRMS map (Figure 4B).

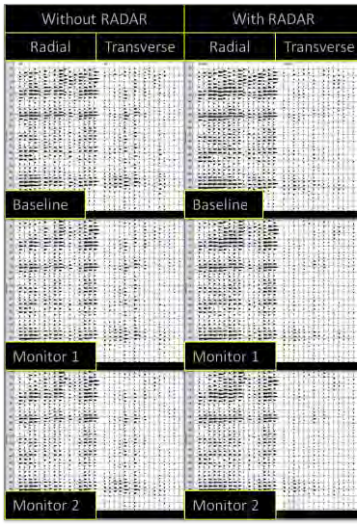

Figure 3. Common receiver stacks along a fixed receiver line for all three vintages (rows), with/without RADAR applied (right/left columns). R and T stacks are shown for each vintage with/ without RADAR. Improvement achieved by applying RADAR is evident as energy has moved from the T onto the R component, enhancing lateral coherence on the R component. Remaining T component energy is due to SWS.

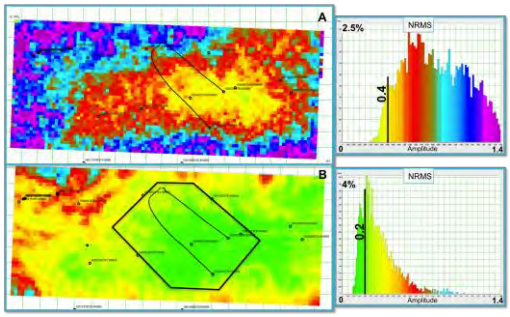

Figure 4. NRMS error (Monitor 1 – Baseline) maps and histograms from final processing product with (B) and without (A) RADAR pre-processing applied. The improvement in repeatability is evidenced by the lower mean and variance in the distribution of NRMS error values. The data analysis polygon outlined on (B) was chosen based on high repeatability above the well locations.

Layer stripping analysis. SWS analysis was conducted on all three vintages. We recommend removal of SWS effects from all layers above the reservoir (e.g. "layer stripping", Gaiser, 1999). Indeed, shear-wave energy reflected from and beyond the zone of interest must pass through all layers above it, arriving at the receivers encoded with these propagation effects. Often, as with Pouce Coupe, the

overburden exhibits strong SWS, confounding information received from the reservoir.

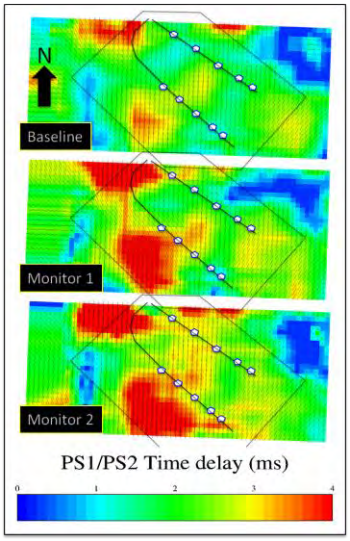

Figure 5. Prestack time-delay and PS1 azimuth estimates after layer stripping to the reservoir level, for all vintages. Wells are drawn along with hydraulic fracture stages indicated by small pentagons. Color scale represents time delays between PS1 and PS2 events, while needle orientation indicates the estimated PS1 azimuths. Gradual background increases in time delay are directly associated with reservoir activity. Orientation changes are negligible.

SWS analysis involves scanning over a range of trial fast and slow (PS1 and PS2) azimuths. For each trial, the data are rotated into the trial PS1, PS2 azimuths, a suite of trial time-delays are used to layer strip the data, and the entire suite is analyzed upon rotation back to R and T coordinates. This analysis involves optimization of an objective function (Silver and Chan, 1991); most current methods rely on minimizing the energy on the transverse component after layer stripping (Li and Grossman, 2012). However, conventional transverse-based methods become unstable due to low signal-to-noise ratios, or when only marginal SWS occurs. We have adopted a more sensible objective of maximizing coherence of shear-wave energy transferred onto the radial component (Li and Grossman, 2012).

Time delay and PS1 azimuth estimates resulting from the layer stripping procedure down to the reservoir level are displayed for all three seismic volumes (Figure 5). The polygon bounds the area of interest, and the horizontal wells are displayed with hydraulic fracture stages indicated by small pentagons. Color scale and needle length represent estimated time delays (SWS magnitude) between PS1 and PS2 events, and needle orientation represents the estimated PS1 azimuths. The maximum SWS magnitude is about 4ms, and a good correlation exists between reservoir activity and regions of increasing time delay, while the PS1 orientations remain quite stable over time.

Montney shale example

The Pouce Coupe 4D 3C surveys were acquired in 2008 to characterize and monitor changes caused by hydraulic fracturing within the unconventional reservoir. The dataset includes a baseline survey acquired after drilling the location's two horizontal NW-SE trending wells (2-07 and 7-07), plus two monitor surveys obtained after each of the two corresponding hydraulic fracture treatments (Figure 1). The horizontal wells have identical drilling and completion parameters, except for the targeted intervals Montney C (2-07) and D (7-07). Due to the proximal location of the field to the Rocky Mountain deformation belt, the stress regime is strongly azimuthally anisotropic, with the maximum horizontal stress being up to 1.8 times the magnitude of the minimum horizontal stress (Heather Davey, 2012). The characteristic tight nature of the Montney reservoir requires flow pathway heterogeneities, such as natural fractures, to be accessed for economical development.

Fracturing of reservoir rock creates azimuthally dependent shear strength, and ultimately the shear velocities to be different parallel and perpendicular to fracture planes. Use of C-waves for near vertical fracture interpretation is encouraging because the orientation of dominant open fractures may be determined and the velocity differential enables fracture density characterization. In comparison, microseismic surveys potentially monitor the volume of reservoir reacted to the hydraulic fracture treatment (stimulated reservoir volume) but little is known how fractures behave when distributing proppant to keep fracture permeability pathways open, ultimately relating to the effective fracture network. This is one application of 3C seismic technology where the use of C-waves for imaging reservoir azimuthal anisotropy shows great promise.

Stacked PS1 and PS2 volumes (Figure 6) allow vertical PS1 and PS2 traveltime differences to be analyzed within the reservoir more precisely. The poststack approach of estimating SWS from time-delays is a horizon-based measurement. SWS magnitude is analyzed from traveltime differences between the PS1 and PS2 poststack images of a known seismic marker at the base of the reservoir, yielding an effective SWS magnitude over the reservoir interval.

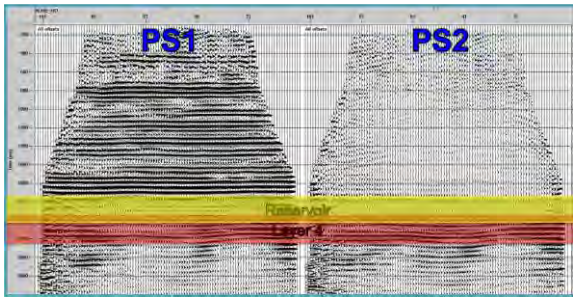

Figure 6. Final stack result of converted-wave data after processing and layer stripping. The reservoir interval is located between 2100-2400 ms (outlined in yellow). The final window for the SWS analysis is shown by layer 4 (2150-2450 ms).

A key part of pre-stimulation reservoir characterization is determining the natural fracture orientations and their density. The baseline characterization shows weak SWS magnitude—less than 3% (Figure 7A). These small values

may be due to non-preferential orientation of open natural fractures. Although the anomalies are small, the SWS maps exhibit two dominant trends oriented northwest and northeast (Figure 7A). Independently, subsurface image log interpretation reveals the Montney formation has two fracture sets, one oriented parallel to the regional maximum horizontal stress direction (north-40-degrees-E) and a perpendicular set (Davey, 2012). Based on the PS1 orientations determined by the layer four SWS analysis (Figure 5), it is observed that the principle fast shear-wave orientation varies over the local field scale and may correspond to the two dominant fracture orientations.

Within Pouce Coupe, the fracture set that is likely to fail from hydraulic completions is observed to vary and is controlled by the dominant natural fracture orientation (Davey, 2012). Predictive fracture failure was determined using Mohr-Coulomb failure theory, the treating pressures seen during stimulation, and the variations likely due to local tectonic reorientations or differential stress cycling history. After the completion of the 2-07 well, three induced SWS anomalies are present (Figure 7B). The linear induced anomaly (NE-SW) at the southern (toe) portion with values between 3 and 5% SWS may be associated with a wrench fault trending parallel to the present-day regional maximum horizontal stress direction (N40E). This minor offset fault is one of many over the survey area that was only possible to interpret using the C-wave data. The SWS anomalies located at the center and heel stages have values between 4 and 7% SWS and build only south of the well bore representing preferential propagation. The dominant orientation of the highest magnitude anomaly is a result of the hydraulic fracture interacting with the perpendicular natural fracture set (NW-SE) and is interpreted as opening fractures against the regional maximum horizontal stress.

Figure 7C shows completion effects of the two horizontal wells. It is believed from the lack of new 4D SWS anomalies near the 7-07 well the majority of the completion energy was lost into open fractures of a previously interpreted wrench fault.

From the microseismic data analysis (not shown here), it was observed that the microseismic events were focused at the toe of the 7-07 well and propagated towards the 2-07 well, supporting the SWS results. The other two anomalies near well 2-07 discussed above decreased in magnitude and became much more diffuse, and may represent the equilibrating of reservoir pressure and the fractures closing on the proppant. The dominant fracture orientations did not change significantly between baseline and monitor surveys (Figure 5), implying that natural faults and fractures controlled displacement of hydraulic completion energy and that induced anomalies may correspond to propping of pre-existing fracture networks.

The final SWS signature may reflect the overall connectivity of the open fracture network. It is interesting to compare the SWS anomalies with the spinner production data collected for each stage perforation location. In Figure 7 B and C, the spinner data are portrayed as percent of total gas flow, which is ultimately related to natural fracture

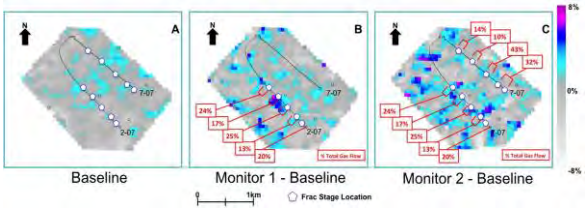

Figure 7. Map view of SWS averaged over the Montney reservoir interval. Spinner production data are highlighted by frac stage and represented as percentage of total gas flow. A: Baseline SWS from time-delays. B: SWS difference between monitor 1 and baseline, after the completion of the 2-07 well. C: SWS difference between Monitor 2 and Baseline, after the total completion of 2-07 and 7-07 (hydraulically fractured and propped). Each pixel represents a 50x50m Asymptotic Conversion Point bin.

permeability and hydraulic stimulation success. Baseline fracture locations and density relate to the success of each hydraulic fracture stage and should be used in completion design (Figure 7A). Induced anomalies are related to hydrocarbon deliverability and are interpreted as propped fractures (Figure 7B, C). From 3C seismic reservoir characterization and monitoring, optimum perforation locations can be determined, yielding an increase of producible gas.

Conclusions

The Pouce Coupe 4D 3C data provide insight into stress and fracture-related reservoir anisotropy through the analysis of SWS. Successful use of C-wave data to distinguish reservoir anisotropy relied on key aspects of the processing sequence, which employed novel methods such as RADAR to better preserve vector fidelity, NRMS-guided simultaneous processing for increased repeatability, and coherence of the radial component as objective function for the layer stripping procedure to increase SWS sensitivity at the reservoir interval. We demonstrated the utility of SWS analysis both on common azimuth stacks and poststack after layer stripping in determining the SWS orientation and magnitude by relating these attributes to the "propping" of fractures.

Acknowledgements

We thank Talisman Energy, especially David D'Amico, for review and permission to show the results. We also thank Rodney Couzens for processing, review, and helpful discussions, Colorado School of Mines, Tom Davis for his leadership and helpful guidance, Heather Davey, David Cho and Bonnie Nasim for proofreading, and Jim Gaiser for inviting us to present this paper, which is based on our 2013 TLE article.